Int. J. Multiphase Flow Vol. 17, No. 1, pp. 13–26, 1991
Printed in Great Britain.

0301-9322/91 $3.00 + 0.00

SMALL AMPLITUDE KINEMATIC WAVE PROPAGATION IN TWO-COMPONENT MEDIA

H. K. KYTÖMAA† and C. E. BRENNEN
Department of Mechanical Engineering, Mail Code 104-44, California Institute of Technology, Pasadena, CA 91125, U.S.A.

(Received 23 October 1989; in revised form 27 June 1990)

Abstract—Experimentally determined attenuation and propagation characteristics are presented for small amplitude concentration waves in vertical bubbly and particulate flows. These were studied up to concentrations of 44.3 and 58%, respectively, in a 10 cm pipe. The wave propagation was studied in terms of the time delay, phase lag and loss of coherence of naturally occurring volume fraction fluctuations by means of simultaneous impedance measurements at two separate locations. Small amplitude natural kinematic waves were confirmed to be non-dispersive, as has previously been shown by other investigators. In this system configuration, bubbly flows undergo a regime transition to churn-turbulence, and not to slug flows as is typically observed in smaller diameter pipes. A dramatic drop in the attenuation time constant of small kinematic waves was found prior to the transition to churn-turbulence in gas–liquid flows, indicating that the regime change is the consequence of a loss of kinematic stability. The solid–liquid mixtures studied were found to always remain stable, with a range of greatest stability between 15–20%, as indicated by a maximum in the kinematic wave attenuation constant. The idea of a stable intermediate range of concentrations is consistent with the observations by Homsy *et al.* [*Int. J. Multiphase Flow* **6**, 305–318 (1980)], who first observed structure formation above and below such a range. At concentrations above 40%, gradual transition to plug flow occurs, in which the particles execute little or no motion relative to one another.

Key Words: bubble, solids, fluidized bed, stability, churn-turbulence, plug

1. INTRODUCTION

While the motion of individual bubbles and particles have been studied extensively [see Wallis (1969) or Clift *et al.* (1978) for a review], the behavior of collections of monodispersed bubbles and particles remain less well understood. Due to the complexity of such flows at high concentrations, they have mostly been studied in terms of averaged quantities, and it is recognized that continuity wave propagation plays an important role in their behavior. These waves were first studied by Kynch (1952) in the context of sedimentation where the interest in their propagation was primarily motivated by the method of analysis, the method of characteristics. This work has since been generalized to inclined flows for the different flow regimes of both gas–liquid and solid–liquid flows (Zuber & Findlay 1965; Wallis 1969).

The kinematics of two-component flows are central to understanding their low frequency behavior and flow stability in the presence of slip. The kinematics of liquid–solid systems have been studied extensively in the context of fluidized beds (Zenz 1971; Homsy *et al.* 1980; Jackson 1985; Batchelor 1988) in an attempt to better understand fluidized bed stability and the causes of "bubble formation". It is generally agreed that the onset of instability is caused by the initial growth of planar concentration waves that, depending on the conditions, may or may not break-up into three-dimensional structures. Disagreement exists regarding the details of the stability criteria in terms of the system parameters, although all recent studies indicate that strong particle–particle interactions have a stabilizing effect. The discussion on the nature of such interactions has previously focused on the experimentally elusive dispersed phase pressure (Jackson 1985; Homsy *et al.* 1980), with inconclusive results. Recently, Batchelor (1988) demonstrated that the dispersed phase diffusion is the dominant factor in kinematic stability.

†Present address: Department of Mechanical Engineering, Massachusetts Institute of Technology, Cambridge, MA 02139, U.S.A.

In gas–liquid systems, both industrial needs, and a vacuum of good data for comparison with developments in models have motivated ongoing efforts. Several recent studies have focused on the propagation of concentration waves in vertical gas–liquid flows (Mercadier 1981; Bernier 1982; Bouré & Mercadier 1982; Pauchon & Banerjee 1986). Using either resistive or beam attenuation techniques, it has been shown that it is relatively easier to measure kinematic wave speeds than their attenuation. The above studies addressed wave propagation in stable bubbly flows in circular and square channel cross sections ranging in linear dimension between 2 and 10 cm. The two studies that have investigated larger concentrations and regime change (Tournaire 1987; Matuszkiewicz *et al.* 1987) limited themselves to small tubes (2.5 cm dia and 2 cm^2, respectively) in which wall shear stresses have an important influence on the nature of the flow and regime transitions. For these channel dimensions, bubbly flows undergo transition to slug flow.

In this study, the propagation and attenuation of natural concentration waves were studied in low superficial velocity solid–liquid and gas–liquid flows in a vertical pipe of much larger diameter than the bubbles or particles. This choice was made to accommodate gas–liquid flows with a transition to churn-turbulence rather than slug flow to complement existing results. Stable bubbly gas–liquid flows were attained up to concentrations of 44.3%, and their behavior was documented up to the transition to churn-turbulence. Similarly, solid–liquid flows were studied up to a solids concentration of 58% and were observed to gradually assume a rigid structure with no relative motion between particles, at concentrations above 40%. In this paper, this regime is called plug flow.

2. EXPERIMENTAL FACILITY

The three-component flow facility (TCFF) used for the solid–liquid and gas–liquid study is shown in figure 1. The test section is a vertical clear acrylic pipe, 102 mm dia and 2.2 m long. Bubbly flows are formed by introducing the gas through an injector situated inside the vertical pipe, 0.5 m below the test section. It consists of an array of 12 3.2-mm dia brass tubes perforated with 0.4 mm holes, located to give a uniform bubble distribution over the cross section. A 0.8 MPa compressed air line supplies the injector through a regulator, an orifice plate flowmeter (to monitor the air mass flow), valves to control the air flow and a manifold to distribute the air flow evenly among the brass tubes.

The solid–liquid mixture consists of water and polyester particles. The facility is able to internally handle the solids and to control their flowrate independently of the liquid without external addition or removal. When at rest prior to an experiment the solids are trapped between a vertical 10 cm control cylinder and the storage hopper (see figure 1). As the control cylinder is raised from the reducer on top of which it sits, the gap created allows particles to enter the test section under the action of gravity. The solids flowrate is varied by adjusting this gap by means of a control rod attached to the cylinder. The solids are recycled after an experiment by fluidization back to the upper hopper where they settle into their original position with the control cylinder in its lowered position.

The mean bubble and polyester particle diameters were 4 mm (± 0.5 mm) and 3 mm (± 0.5 mm), respectively. Only low flowrates were studied; the liquid fluxes of all two-component flows considered were no larger than 0.2 m/s.

The volume fraction of the dispersed medium is measured using a non-intrusive impedance volume fraction meter (IVFM). It operates on the same principle as the one developed by Bernier (1982) and has been equiped with temperature compensation and a shielded electrode configuration to decrease the axial extent of the measuring volume. The active stainless steel electrodes (6.4 mm high) are flush mounted into a section of 102 mm dia non-conducting acrylic pipe, and form diametrically opposed 90° arcs on the circumference of the pipe. The active electrodes are each sandwiched between two shielding electrodes. These are 9.5 mm in axial length and also form 90° arcs. Figure 2 shows the electrode configuration. The shielding electrodes duplicate the active electrode potential through a high input impedance voltage follower. The IVFM is excited at an amplitude of 0.3 V r.m.s. and a frequency of 40 kHz at which the impedance is found to be primarily resistive. The active electrode pair is connected in a bridge configuration. Its offset voltage is demodulated by multiplication to the driving signal, followed by removal of the 80 kHz signal using a low-pass filter. The remaining low frequency signal is caused by fluctuations in the volume

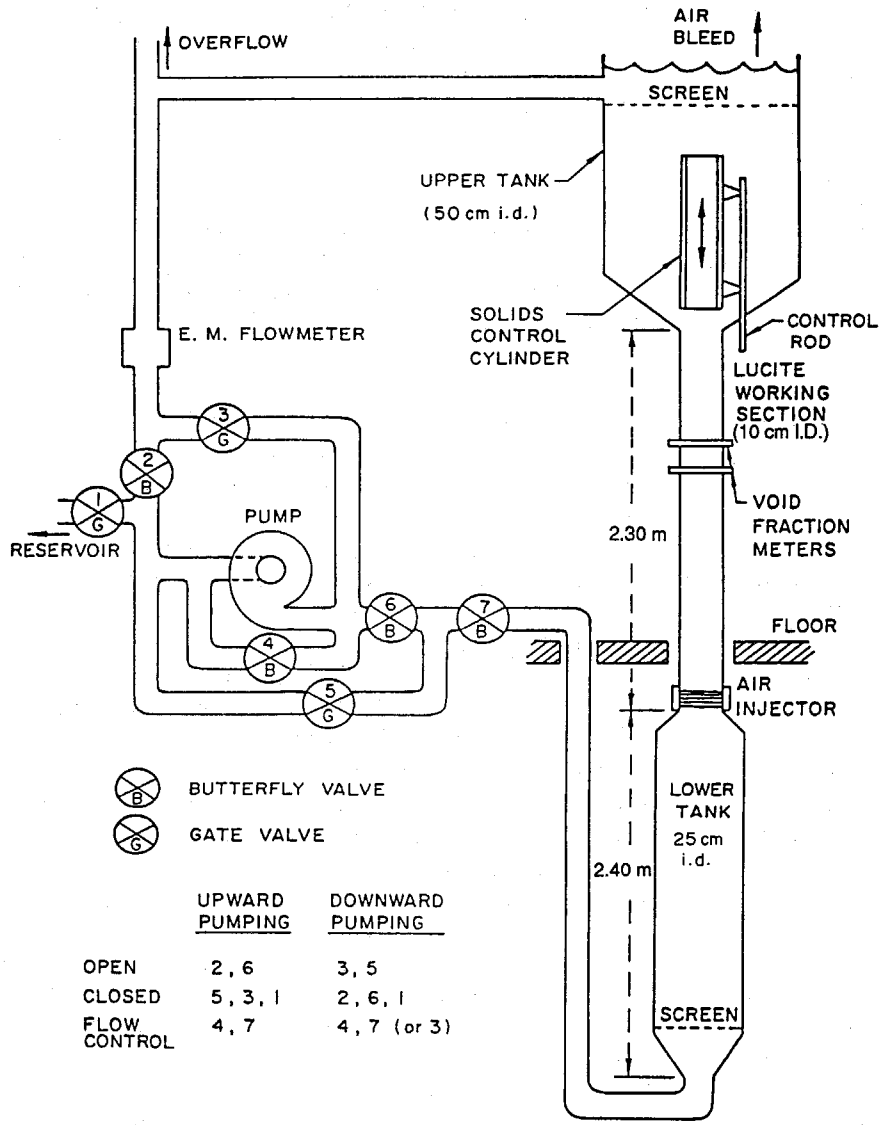

Figure 1. Schematic of the three-component flow facility.

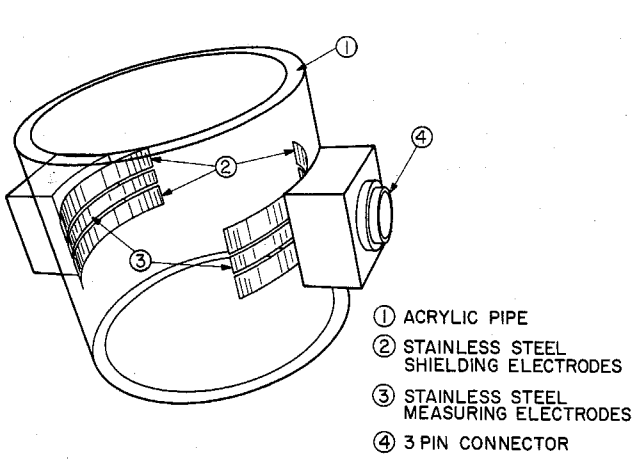

Figure 2. Isometric view of the shielded impedance volume fraction meter electrode geometry.

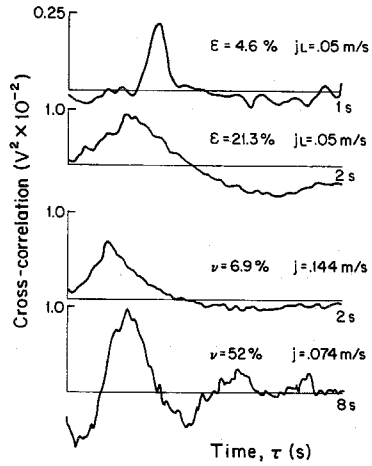

Figure 3. Typical cross-correlations of the IVFM output fluctuating voltage in bubbly and particulate flows.

fraction. The IVFM has excellent linearity for both bubbly and particulate flows up to volume fractions of 50%, as shown by hydrostatic calibration at low liquid superficial velocities (Kytömaa & Brennen 1988). With a sensitivity of 0.15 V/percent of volume fraction, the passage of individual bubbles (or particles) is readily detectable.

3. THE CROSS-CORRELATION FUNCTION AND ITS INTERPRETATION

By means of a dynamic calibration in which the passage of individual particles (or bubbles) is modeled as a random shot noise process, it was established that the spatial resolution of the IVFM is of the order of 1 cm in the axial direction (Kytömaa 1987; Kytömaa & Brennen 1988), and that the influence volume of the measurement remains unchanged for all volume fractions and flowrates considered. These properties make the IVFM suitable for the study of volume fraction perturbations over a broad range of wavelengths and allow the IVFMs to be used close to one another without the problem of cross-talk. Measurements of the fluctuations in the volume fraction signal were made simultaneously at two closely spaced locations (separation, $h = 0.0735$ m) under steady flow and volume fraction conditions for both bubbly and particulate flows.

The IVFM fluctuating component was obtained by passing the IVFM output signal through a high-pass filter with a 3 dB cutoff frequency of 0.032 Hz and a fall off slope of 10 dB/octave. The filter output was recorded on magnetic tape for reduction. The record lengths were as long as 20 min for bubbly flow measurements and no shorter than 1 min for particulate flows. Cross-correlations of simultaneously recorded data from the two IVFMs were obtained on an HP 3562a signal processor. Repeatable cross-correlograms were obtained by ensemble averaging the measurements with ensembles ranging in length between 1–10 s. These yielded the residence time of coherent waves between the two concentration transducers. Typical measured cross-correlation records are shown in figure 3. The residence time, τ_{max}, is obtained from the location of the peak in the cross-correlograms. Knowing the time taken by the coherent signal to travel from one IVFM to the other, and the distance, h, between the electrode pairs, we calculate the speed of propagation information, v_X in the two-component flows in question:

$$v_X = \frac{h}{\tau_{max}}. \qquad [1]$$

This propagation velocity is shown as a function of the volume fraction of the dispersed phase in figure 4 for bubbly flows and in figure 5 for solid–liquid flows. These speeds are compared with the infinitesimal kinematic wave velocities, shown as a solid curve, obtained using the drift flux model (Zuber & Findlay 1965; Zuber & Staub 1966; Wallis 1969). This confirms that the velocity obtained with this cross-section correlation method is the kinematic wave speed as intended, not the speed of the dispersed inclusions.

Indeed, the cross-correlation of point volume fraction measurements as obtained with hot film anemometers or fiber optic probes separated by a small distance (of the order of the diameter of the dispersed medium) typically yields the dispersed medium (bubble) velocity. The

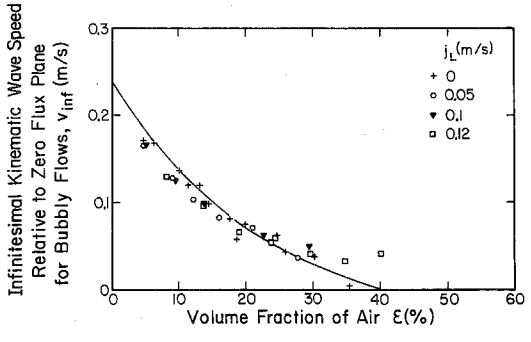

Figure 4. Infinitesimal kinematic wave speed values obtained by the cross-correlation technique for bubbly flows. The solid curve is the infinitesimal kinematic wave speed based on the drift flux model and measurements of the air drift flux.

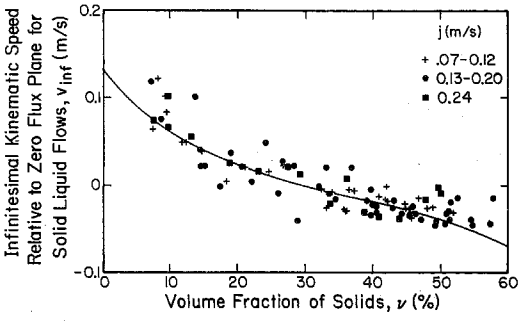

Figure 5. Infinitesimal kinematic wave speed values obtained by the cross-correlation technique for particulate flows. The solid curve is obtained using the drift flux model.

cross-correlation based speeds were also compared to the bubble and particle speeds to confirm that v_X was the kinematic velocity. The bubble speed relative to the liquid is obtained from the measured air and water fluxes (j_G and j_L) and the volume fraction, ε, using

$$v_G = \frac{j_G}{A\varepsilon} - \frac{j_L}{A(1-\varepsilon)}. \qquad [2]$$

In polyester particle–water flows the particle velocity relative to the water was obtained indirectly by measuring the propagation speed of finite kinematic shocks. This method was tested with bubbly flows and showed to be a consistent method of determining the disperse medium velocity.

The results eliminate the ambiguity in the interpretation of our measurements and confirm that the cross-correlation of the volume fraction fluctuations (as measured using the IVFMs) yields the speed of infinitesimal kinematic waves for bubbly and solid–liquid flows. These findings agree well with those of other investigators (Mercadier 1981; Bernier 1982; Bouré & Mercadier 1982; Pauchon & Banerjee 1987; Matuszkiewicz *et al.* 1987; Tournaire 1987; Saiz-Jabardo & Bouré 1989).

4. THE NON-DISPERSIVE NATURE OF INFINITESIMAL KINEMATIC WAVES

In this section we turn our attention to the propagation and attenuation of structure in vertical two-component flows. A measure of the structure is obtained from the statistical properties of the fluctuations in the volume fraction signal. The continuous reordering of the disperse species in the stable steady two-component flows observed is represented below in terms of attenuation of the coherent signal from one IVFM to the other. The power spectra of volume fraction fluctuations at two different locations in a kinematically stable flow were found to be consistently equal within the inherent noise level of the spectra. Experimentally obtained power spectra demonstrate this feature in figure 6 for two different values of the volume fraction for bubbly flows. In the present results, only flows that exhibited no change in the power spectrum from one measuring station to the other were considered. Therefore, the amplitude of the uncorrelated component of the signal at the downstream location must be equal to the attenuated component of the coherent signal, to remain consistent with the constant power spectra at the two IVFMs. In general, both the attenuation of the kinematic waves and their residence time between the IVFMs depend on the wavenumber. For this reason, the model is best presented in the frequency domain. For kinematic waves traveling from IVFM1 to IVFM2, the Fourier-transform of the measured fluctuations can therefore be written as

$$\tilde{V}_1(\omega) = \frac{1}{2\pi}\int_{-\infty}^{\infty} e^{-i\omega t}\tilde{V}_1(t)\,dt \qquad [3]$$

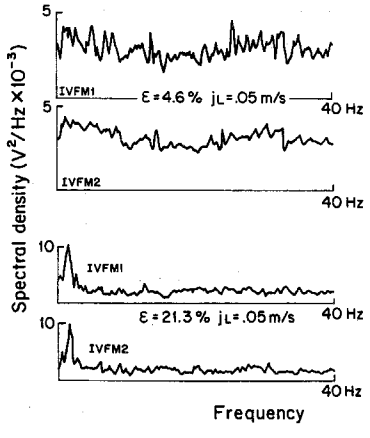

Figure 6. Power spectra of the IVFM output fluctuating voltage measured simultaneously at two locations separated by 0.0735 m, for bubbly flows.

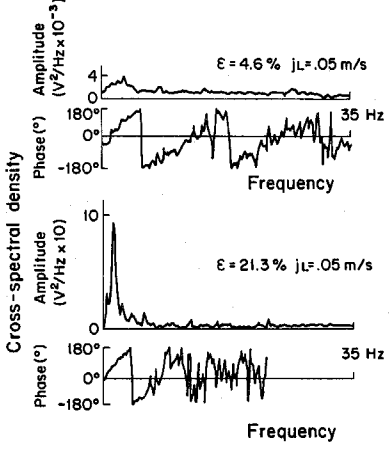

Figure 7. Cross-power spectrum of the IVFM output fluctuating voltage at two locations separated by 0.0735 m, for bubbly flows showing the linear relation between phase and wavenumber for wavenumbers at which the signal is significant.

and

$$\tilde{\mathbf{V}}_2(\omega) = \zeta(\omega)\mathrm{e}^{-i\omega T(\omega)}\tilde{\mathbf{V}}_1(\omega) + \tilde{\mathbf{V}}_{2R}, \quad [4]$$

where $\zeta(\omega)$ is the wavenumber dependent attenuation (or gain if >1) and $T(\omega)$ is the transit time of the perturbation of frequency ω between the two detector positions. The factor $\mathrm{e}^{-i\omega T(\omega)}$ is the characteristic "time delay exponential" which arises when taking the Fourier-transform of a signal with a time lag $T(\omega)$. The quantity $\tilde{\mathbf{V}}_{2R}$ is the fluctuating term which is not correlated with $\tilde{\mathbf{V}}_1$.

To evaluate the wavenumber dependence of the kinematic velocity, we determine the delay time dependence on the wavenumber. The cross-power spectrum of the fluctuations of IVFM1 and IVFM2 contains this information in its phase. The cross-power spectrum of the two signals is

$$S_{\tilde{\mathbf{V}}_1\tilde{\mathbf{V}}_2} = \tilde{\mathbf{V}}_1^*(\omega)\tilde{\mathbf{V}}_2(\omega), \quad [5]$$

where a superscript $*$ denotes the complex conjugate. Substituting [4] into [5] we obtain

$$S_{\tilde{\mathbf{V}}_1\tilde{\mathbf{V}}_2} = \zeta(\omega)\mathrm{e}^{-i\omega T(\omega)}S_{\tilde{\mathbf{V}}_1\tilde{\mathbf{V}}_1}, \quad [6]$$

where $S_{\tilde{\mathbf{V}}_1\tilde{\mathbf{V}}_1}$ is the power spectrum of the fluctuations of IVFM1,

$$S_{\tilde{\mathbf{V}}_1\tilde{\mathbf{V}}_1} = \tilde{\mathbf{V}}_1^*(\omega)\tilde{\mathbf{V}}_1(\omega). \quad [7]$$

Since the power spectrum $S_{\tilde{\mathbf{V}}_1\tilde{\mathbf{V}}_1}$ is a real function, it follows that the phase $\phi(\omega)$ of the cross-power spectrum in [6] is

$$\phi(\omega) = -\omega T(\omega). \quad [8]$$

The cross-power spectrum phase, $\phi(\omega)$, was evaluated for the recorded experimental data. Typical results are shown in figure 7. The phase was found to be linear in ω in the region where the cross-power spectrum amplitude is significant, for both bubbly and particulate flows. The independence of $T(\omega)$ on the frequency ω confirms that naturally occurring kinematic waves are non-dispersive, as has been shown by others [see Jackson (1985) for solids and Saiz-Jabardo & Bouré (1989) for bubbles], and the slope of the phase was found to be consistent with measured residence times. This validates the use of the cross-correlation in determining small amplitude kinematic speeds, and makes it a valuable tool in determining the attenuation time constant of kinematic waves, as shown in the following section. Since all wavelengths travel at the same speed we can represent the frequency in terms of a more physical quantity, namely the wavenumber N, which is related to the frequency through the following equation:

$$N = \frac{\omega}{v_X}, \quad [9]$$

where v_X is the kinematic wave speed.

5. THE ATTENUATION OF SMALL AMPLITUDE KINEMATIC WAVES

The main motivation behind shielding the electrodes of the IVFM was to improve the spatial resolution of the device, thereby allowing us to study the properties of short wavelength infinitesimal kinematic waves (<0.1 m) which have eluded many authors due to the large geometry of their measuring devices. This was successfully accomplished, as indicated by the power spectra in figure 6 which contain wavelength information down to 0.05 m.

We now seek the attenuation of infinitesimal kinematic waves as a function of the wavenumber. This is readily obtained from the gain factor $H(N)$ defined below. It is <1 if the waves are attenuated and >1 if they grow. Under the conditions of invariant power spectra, $H(N)$ is equal to the coherence function, $\gamma(N)$:

$$H(N) = \frac{|S_{\tilde{\mathbf{V}}_1\tilde{\mathbf{V}}_2}|}{S_{\tilde{\mathbf{V}}_1\tilde{\mathbf{V}}_1}} = \gamma(N) = \frac{|S_{\tilde{\mathbf{V}}_1\tilde{\mathbf{V}}_2}|}{\sqrt{S_{\tilde{\mathbf{V}}_1\tilde{\mathbf{V}}_1}S_{\tilde{\mathbf{V}}_2\tilde{\mathbf{V}}_2}}}. \quad [10]$$

In the present experiments, coherent information is always attenuated and therefore, $\gamma(N)$ is always <1. It can be verified that the signals from the two measuring locations contained no coherent external noise unrelated to the phenomenon of interest from the nature of the cross-correlograms of the two channels. In the presence of such parasitic noise these would reveal peaks in the cross-correlation close to $\tau = 0$, which were never observed. Substituting for $S_{\bar{v}_1\bar{v}_2}$ from [6] we get

$$\gamma(N) = \zeta(N). \qquad [11]$$

The coherence function is identical to the previously defined attenuation. Results for both bubbly and particulate flows are shown in figures 8 and 9. These are shown in terms of a reduced wavenumber, n, which is defined as $n = ND$, where D is the mean diameter of the dispersed phase. For both types of flows, these show an increased persistence in volume fraction fluctuations as the volume fraction is increased, but they never reach an unstable state, and the coherence remains <1.

5.1. Attenuation of fluctuations

Since the kinematic wave speed varies as a function of the mean volume fraction (figure 3), a general representation of the attenuation of small waves can be made in terms of coordinates following the wave rather than fixed laboratory coordinates, as used by Saiz-Jabardo and others. Assuming that the waves are attenuated exponentially, we write

$$\gamma(N) = e^{-k(N)T}, \qquad [12]$$

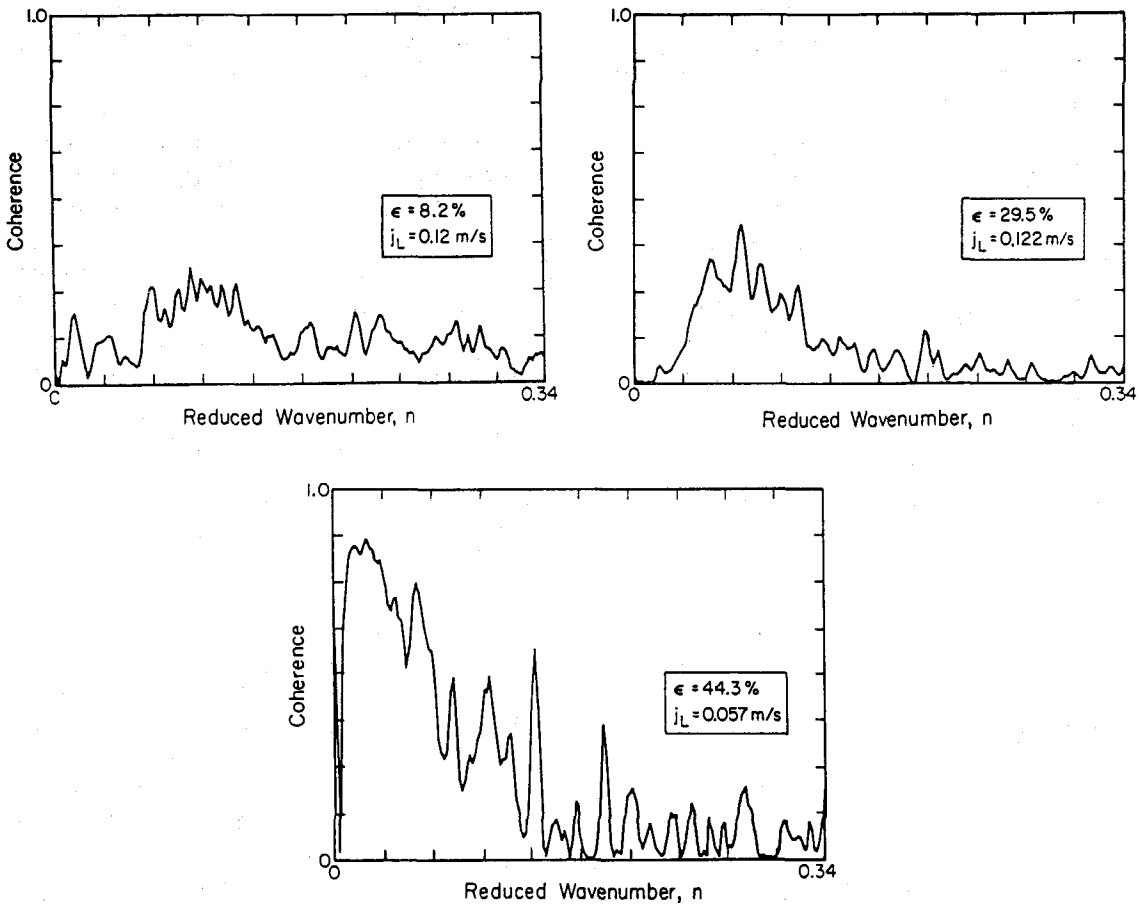

Figure 8. Coherence of the two IVFM fluctuating output signals (separation of IVFMs = 0.0735 m) in bubbly flows plotted against reduced wavenumber.

where k is the wavenumber dependent attenuation time constant of infinitesimal kinematic waves and T is the residence time of the wave between the two measuring locations. This linear form is valid for small fluctuations in the volume fraction signal, which is the case here since the system is stable and fluctuations die away, i.e. $k > 0$. Taking the natural logarithm of [12] yields

$$k(N) = -\frac{1}{T}\ln[\gamma(N)]. \qquad [13]$$

The delay time T is known from the cross-correlation analysis. This equation provides a way of determining the attenuation relation, $k(N)$, from the existing coherence information. The number $k(N)$ is always positive and for convenience it is presented in reduced form in figures 10 and 11 for bubbles and solids, respectively. The reduced attenuation time constant is defined as

$$\kappa = \frac{kD}{V_0}, \qquad [14]$$

where V_0 is the terminal velocity of a bubble or particle relative to the continuous medium at zero volume fraction.

The measurements of all flow conditions investigated were reduced to this form. The reduced attenuation time constants curves all exhibit similar features. Although all wavenumbers are attenuated, there is always a least-attenuated wavenumber. In the following section, the magnitude of the minimum attenuation and the corresponding wavenumber are discussed in detail.

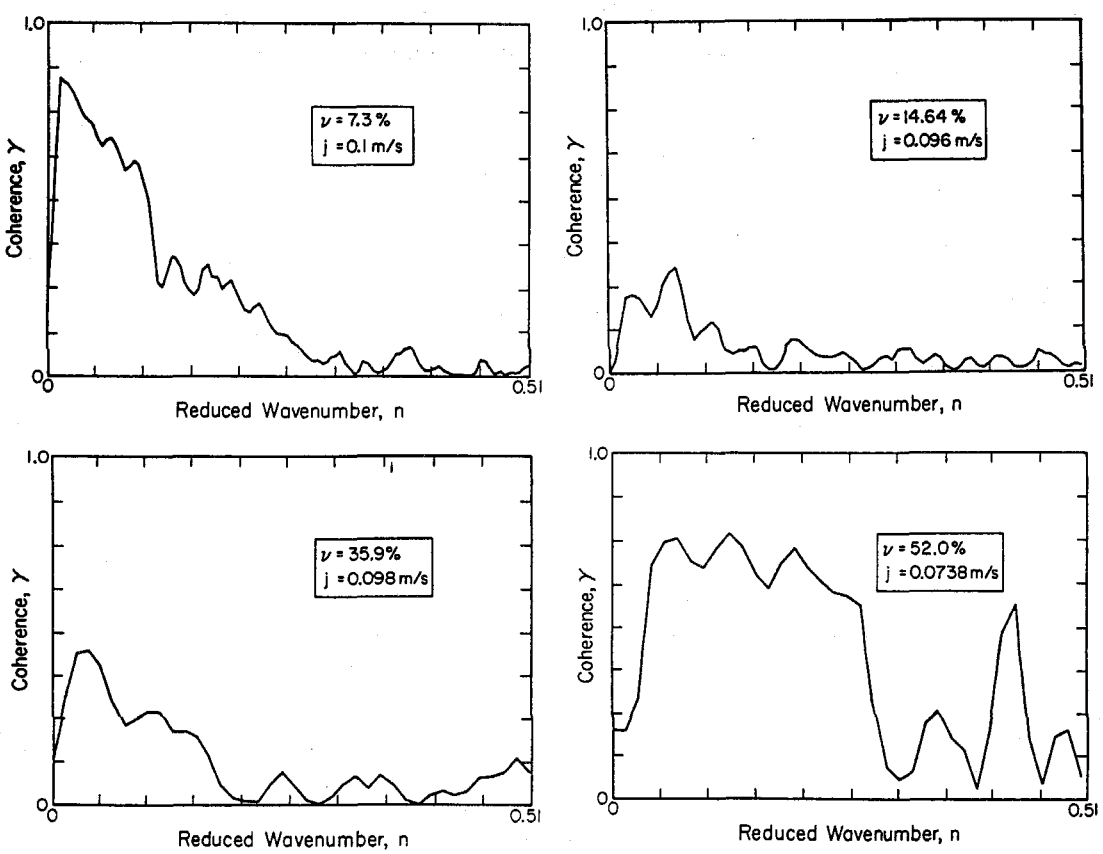

Figure 9. Coherence of the two IVFM fluctuating output signals (separation of IVFMs = 0.0735 m) in particulate flows.

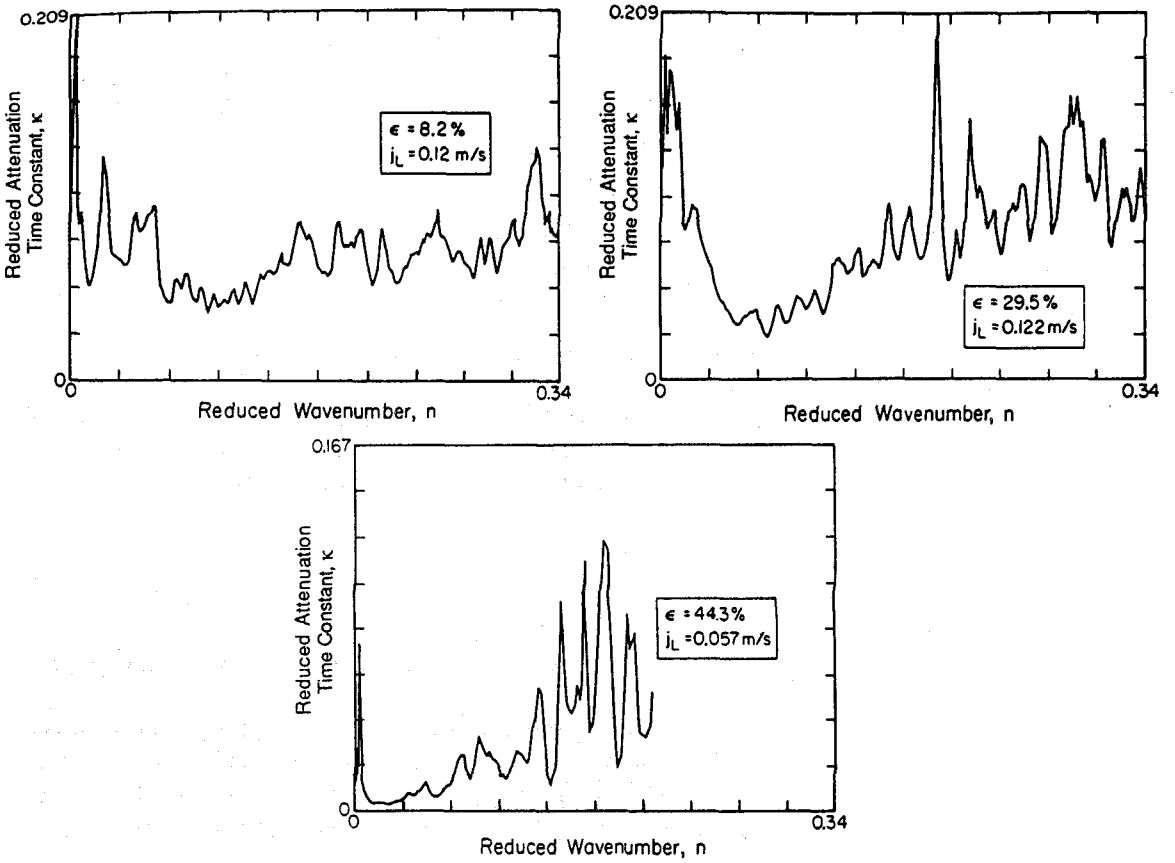

Figure 10. Reduced attenuation time constant calculated from the coherence for bubbly flows, showing a characteristic minimum representative of the least stable wavenumber. Note the decrease in the minimum value at high volume fraction ($\sim 40\%$) prior to the onset of churn-turbulence.

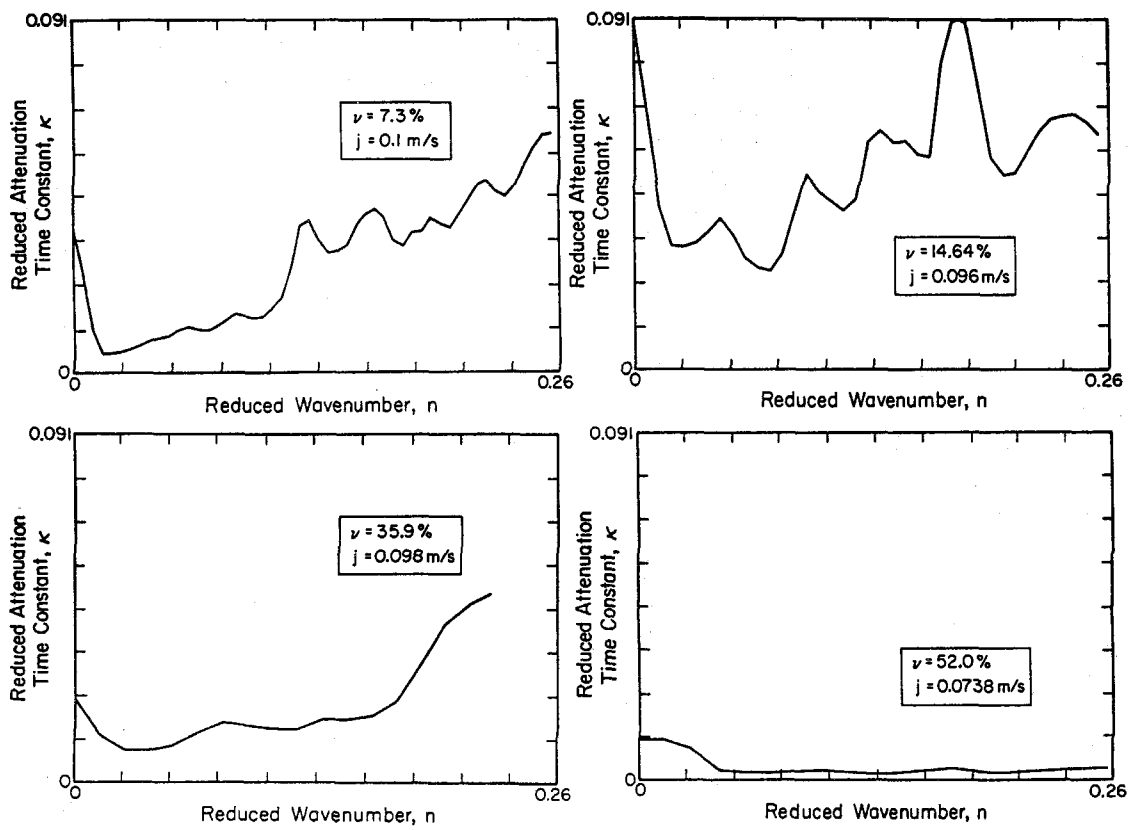

Figure 11. Reduced attenuation time constant calculated from the coherence for particulate flows, showing a characteristic minimum representative of the least stable wavenumber. Note the broad band decrease in the attenuation time constant at high volume fractions, indicative of the tendency of the medium to conserve its structure.

6. RESULTS AND DISCUSSION

6.1. Error analysis

For all volume fractions of both bubbly and particulate flows, the coherence function exhibits a peak which corresponds to the most persistent wavenumber. These experimental coherence traces contain some scatter in the form of non-repeatable fluctuations. Prior to presenting these measurements, it is appropriate to discuss the magnitude and source of this error. It is due to the finite length of our records, and is inversely proportional to the square root of the number of ensembles, n_e. Hence, for the best results, one should maximize the number of ensembles and the duration of the experiments themselves. Due to their batch nature, the solid–liquid flows were limited in duration, and the solids reservoir was depleted more rapidly at high concentrations and high flows. The shortest flow duration was 1 min, while, for comparison, the duration of all bubbly experiments was at least 20 min. In terms of coherence amplitude and the number, n_e, of ensembles, the error in coherence $\delta\gamma$ can be written as

$$\delta\gamma = \frac{[1-\gamma^2]}{\sqrt{2\gamma^2}} \frac{1}{\sqrt{n_e}}, \qquad [15]$$

according to which, the fractional coherence error decreases at high coherences. This is also evident in the experimental coherence "noise level"; the random error is larger at low coherences. Since we are most interested in persistent and hence high coherence waves, the "noisy" least significant data are of little interest to us. The above equation yields an estimate of the random error of 0.21 for the shortest records ($n = 100$, $\gamma = 0.5$ for particulate flows), and of 0.061 for the longest records ($n = 1200$, $\gamma = 0.5$ for liquid flows). The error in the time constant, which is algebraically derived from the coherence, is

$$\frac{\delta k}{k} = \frac{\delta\gamma}{\gamma \ln(\gamma)} + \frac{\delta T}{T}, \qquad [16]$$

where T is the delay time between the two measuring stations. From the cross-correlation data, $\delta T/T$ is estimated at 0.05 for bubbly flows and 0.2 for the shorter duration particulate flows. From these estimates, the compounded maximum error in the time constant k was computed:

$$\left.\frac{\delta k}{k}\right|_{\gamma=0.5} = 0.64 \qquad \text{for solid–liquid flows} \qquad [17]$$

and

$$\left.\frac{\delta k}{k}\right|_{\gamma=0.5} = 0.18 \qquad \text{for bubbly flows.} \qquad [18]$$

It should be noted that these errors are very sensitive to the actual value of γ, and decrease dramatically with higher coherence.

6.2. Gas–liquid flows and the transition to churn-turbulence

According to the coherence measurements, the minimum attenuation time constant is found to undergo a gradual decrease up to an air volume fraction of 40%, as shown in figure 12. Upon a further increase in the volume fraction, κ decreases abruptly from a value of 0.03 to <0.003 at 44.3%, while the flow remains bubbly and uniform with no visible fast, large-scale structures. This sudden fall in κ is accompanied by a shift in the most persistent wavenumber n_{min} from 0.07 to 0.03, as shown in figure 13. These values correspond to kinematic perturbation wavelengths of 0.3 and 0.8 m, respectively, which are large in relation to the pipe diameter of 102 mm.

Upon a further increase in the air flux, in an attempt to reach a bubbly flow concentration of 45%, large fast rising structures become visible, the flow takes on an agitated nature and the volume fraction immediately drops to a value of approx. 35%, indicating that the mean gas velocity has suddenly risen. Transition to *churn-turbulence* has occurred. If we were to extrapolate the

experimental κ curve for larger values of the volume fraction, κ would cross the horizontal axis at $\varepsilon \approx 45\%$. This coincides very closely with the concentration at which the regime change is first observed. These results suggest that the observed onset of churn-turbulence is the consequence of the loss of stability of the small ambient perturbations in the volume fraction. This stability sets in at the wavenumber where the attenuation time constant curve meets the wavenumber axis. According to figure 13, this reduced wavenumber is 0.03. The flow undergoes a regime transition at a concentration of 45%. In the new flow regime, which is a non-linear manifestation of the instability, it is impossible to experimentally infer wave attenuation time constants of higher concentrations, but if the variation of the attenuation curves continues along the same trend, the small amplitude analysis indicates that higher gas volume fraction mixtures may be unstable over a range of wavenumbers and concentrations.

To summarize the attenuation results of the present experiments on bubbly flows, table 1 shows the dimensional attenuation time constant k (s^{-1}) for three values of the void fraction as a function of the wavelength λ of the perturbation.

The only other comprehensive collection of attenuation data for stable bubbly flows available is in Tournaire's (1987) doctoral thesis, for a 25 mm pipe with imposed perturbations. His data are summarized in a similar form in table 2.

In this smaller system, the highest concentration attained for stable bubbly flows was 30.6%, above which transition occurred.

At low concentrations, the attenuation is generally greater for smaller wavelengths. The first distinct difference between the two systems is the noticeably lower attenuation constants k observed at low to intermediate void fractions in the 25 mm pipe. For concentrations $<20\%$, the difference is an order of magnitude below the present values.

Prior to transition at $\varepsilon = 0.255$, Tournaire (1987) also found a drop in the attenuation constant k, and unlike his at low ε, k assumes a minimum which indicates that there is a wavelength that is the most persistent. He found this wavelength to be 0.55 m, which is shorter than the corresponding value of 0.8 m in the current system.

The two systems yield markedly different quantitative results, while they exhibit similar qualitative behavior. Tournaire's results show that for stable bubbly flows, axial variations in propagation speed and attenuation are minimal, hence these differences cannot be attributed to entrance or flow development effects. On the other hand, the two systems have approximately the same bubble size, while Tournaire's pipe is a quarter of the current one in diameter. This strongly suggests that the wall effect, which can be represented in terms of the ratio $D_{\text{bubble}}/D_{\text{pipe}}$, plays a major role in the attenuation of kinematic waves, and a better understanding of the effects of this parameter is needed.

6.3. Solid–liquid flows and the transition to plug flow

The attenuation data for solid–liquid flows are plotted in figures 14 and 15. Their behavior deviates from the bubbly flow findings, and they do not undergo a change in flow regime in the sense discussed above. The minimum attenuation time constant κ is plotted against the solid volume

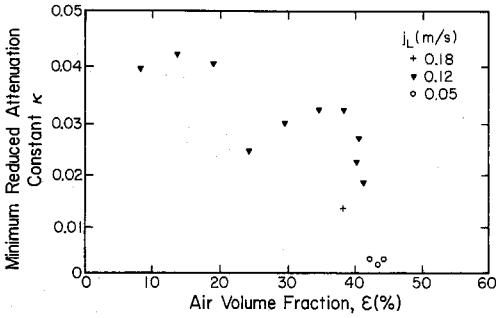

Figure 12. Minimum attenuation constant of bubbly flows of various volume fraction and flowrate conditions presented vs volume fraction. Note the sudden decrease in this variable at $\varepsilon = 40\%$ prior to the onset of churn-turbulence.

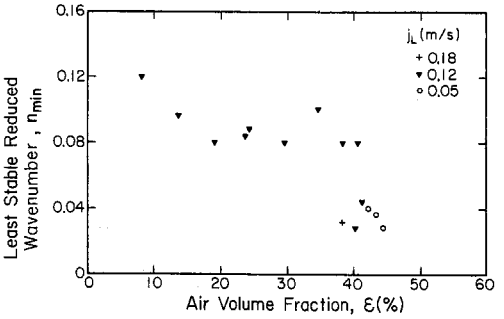

Figure 13. Most coherent wavenumber in bubbly flows of various volume fractions and flowrates.

fraction for the three groups of total flux, which describe the same behavior. They all have a maximum at $v \approx 15$–20%. In this range of solids concentration therefore, fluctuations in the volume fraction are attenuated the most rapidly, and the mixture is most stable. At higher volume fractions ($>20\%$), the attenuation constant κ gradually decreases from a maximum of 0.025 to 0.0015 at $v = 55\%$. This gradual decrease, which differs from the sudden drop experienced with the bubbly flows asymptotes to the horizontal axis. There, the flow assumes a plug-like nature in which no relative motion between the particles can be observed, although the particles remain supported by the fluid at all times (no bridging), as verified by measurements of the vertical liquid pressure gradient. For a plug flow, the IVFM signals at the two monitoring locations become progressively similar but for an inherent time lag. The corresponding attenuation constant would then tend to 0 for all wavenumbers (coherence of 1). Even though the highest flows considered were not true plug flows, low values of κ (<0.003) were obtained for flows with $v \geqslant 40\%$. Consistent with the onset of plug flow is the drop in κ for all wavenumbers at the higher volume fractions.

The most favored wavenumber, $n_{\min}$, assumes values of 0.04 ± 0.02 for solid fractions up to 40%, corresponding to wavelengths of 0.5 ± 0.25 m. At higher concentrations at which broad band persistence of volume fraction fluctuations becomes evident, the minimum in the attenuation time constant becomes less well-defined, and $n_{\min}$ ceases to provide useful insight.

In summary, the ability of the particles to withstand particle–particle forces has a stabilizing effect at high volume fractions and no distinct change in the flow regime takes place. This is in contrast to bubbly flows of high air volume fraction, in which the bubble shape cannot be maintained and close encounters between bubbles lead to coalescence and a regime change.

7. CONCLUSION

In this paper, the dispersion and attenuation relations for kinematic wave propagation were determined experimentally for vertical kinematically stable monodispersed bubbly and particulate flows. This study was limited to low flow velocities and a large hydraulic diameter pipe (10 cm) in comparison with the tubes used in other air–water studies and thin two-dimensional fluidized beds used in particulate fluidization studies. The measurements were based on naturally occurring fluctuations in the volume fraction, and it was confirmed that all measurable perturbations were non-dispersive. Based on the measurements, the attenuation time constant of traveling concentration waves was calculated in terms of a reference frame moving with the wave. The results in relation to observations of flow nature are discussed below.

7.1. *Bubbly flows*

Stable bubbly flows were sustained up to an unusually high volume fraction of 44.3%, above which the flow underwent transition into the churn-turbulent regime. The following conclusions can be drawn regarding the wave propagation results:

- The attenuation time constant gradually decreases up to a gas volume fraction of 40%, above which it takes a sharp drop and, if extrapolated, it reaches zero at

Table 1. Dimensional kinematic wave attenuation constant κ for stable bubbly flows in a vertical 102 mm pipe[a]

$\varepsilon = 0.082$		$\varepsilon = 0.295$		$\varepsilon = 0.44$	
λ(m)	$k(s^{-1})$	λ(m)	$k(s^{-1})$	λ(m)	$k(s^{-1})$
1.25	4.7	1.48	6.0	2.50	0.60
0.23	2.6	0.37	1.8	1.26	0.24
0.15	4.5	0.19	3.8	0.37	0.84

[a]This quantity is presented as measured by an observer following the wave. κ is given for three values of void fraction, as a function of the wavelength λ. These data show the drop in attenuation at the wavelengths which are the most persistent.

Table 2. Dimensional kinematic wave attenuation constant κ, computed from the gain factor data for stable bubbly flows in a 25 mm circular pipe; data taken from Tournaire's (1987) doctoral thesis[a]

$\varepsilon = 0.047$		$\varepsilon = 0.123$		$\varepsilon = 0.255$	
λ(m)	$k(s^{-1})$	λ(m)	$k(s^{-1})$	λ(m)	$k(s^{-1})$
0.44	0.095	0.52	0.10	0.88	0.140
0.31	0.340	0.32	0.18	0.55	0.000
0.17	0.450	0.17	0.39	0.45	0.072

[a]κ is presented as measured by an observer following the wave. These data show a monotonic decrease in κ with λ at the lower void fractions, and a minimum in attenuation at the most persistent wavelength prior to the flow regime transition.

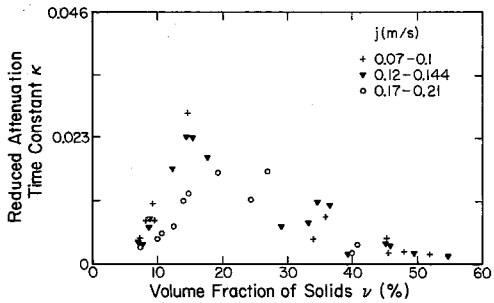

Figure 14. Minimum attenuation constant of particulate flows of various volume fractions and flowrates. The gradually decreasing attenuation constant reflects an increased persistence of structure in the flow.

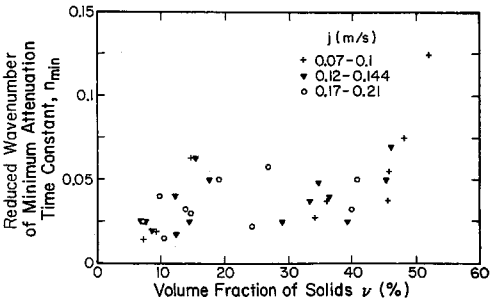

Figure 15. Most coherent wavenumber in particulate flows of various volume fractions and flowrates.

$\varepsilon = 45 \pm 0.5\%$. This coincides with an observed change in regime close to the same value (45%). These two findings provide strong evidence for the view that the regime change is a consequence of the loss of kinematic instability. This idea has been suggested previously by Matuszkiewicz *et al.* (1987) in the context of regime change from bubbly flow to slug flow in a small square channel ($2 \times 2\,\text{cm}^2$), but it has not been demonstrated for the transition to churn-turbulence in larger pipes.

- The most persistent wave length is observed to increase from 0.3 m at $\varepsilon = 10\%$ to 0.8 m at $\varepsilon = 44.3\%$. This large wavelength is the first to become unstable, and its growth results in the transition to churn-turbulence.

7.2. Solid–liquid flows

Vertical downward solid–liquid flows were studied up to a volume fraction of 56%. These did not develop any instabilities but at high concentrations ($\nu = 40\%$) a gradual transition to plug flow occurred, while the solids always remained suspended in the fluid (no bridging). This was ensured by means of pressure gradient measurements. The most persistent perturbation wavelength remained approximately constant at 0.5 ± 0.2 m up to $\nu = 40\%$. Above this concentration all wavelengths become gradually more coherent. This is a consequence of the rigid structure of plug flow, and not an indication of a gradual loss of stability.

The minimum attenuation of perturbations following the wave exhibits a repeatable and distinct non-monotonic pattern with respect to solids concentration. It has a maximum between 15–20%, indicating that the dispersed mixture (excluding plug flows) is the most stable in this range of concentrations. The time constant falls off more sharply at lower rather than higher concentrations, at which it asymptotes to zero as plug flow sets in. An account of similar behavior was only found in one published article. Didwania & Homsy (1981) observed that in a two-dimensional fluidized bed, visible horizontal kinematic waves propagated up the bed at high concentrations. With a decrease in the bed solids fraction (increase in fluidization flowrate) the instabilities disappeared, to reappear at yet lower solids fractions in the form of "bubbles" that were small in relation to the observed waves.

This study demonstrates the difference between bubbly and particulate flows at high concentrations. The rigidity of solid particles, and hence their ability to sustain forces without appreciable deformation, has a noticeable stabilizing effect which leads to the formation of plug flow. Bubbles, which are only held together by surface tension, do not have the mechanism to resist kinematic instability, and consequently undergo transition to churn-turbulence. These results are consistent with the findings of Homsy *et al.* (1980), Jackson (1985) and Batchelor (1988), that show that sustainable particle–particle interactions that do not result in particle agglomeration or coalescence have a stabilizing effect.

REFERENCES

BATCHELOR, G. K. 1988 A new theory of the instability of a uniform fluidized bed. *J. Fluid Mech.* **193**, 75–110.

BERNIER, R. N. 1982 Unsteady two-phase flow instrumentation and measurement. Ph.D. Thesis, California Inst. of Technology, Pasadena.

BOURÉ, J. A. & MERCADIER, Y. 1982 Existence and properties of flow structure waves in two-phase bubbly flows. *Appl. scient. Res.* **38,** 297–303.

CLIFT, R., GRACE, J. R. & WEBER, M. E. 1978 *Bubbles, Drops and Particles.* Academic Press, New York.

DIDWANIA, A. K. & HOMSY, G. M. 1981 Flow regimes and flow transitions in liquid fluidized beds. *Int. J. Multiphase Flow* **7,** 563–580.

HOMSY, G. M., EL-KAISSY, M. M. & DIDWANIA, A. K. 1980 Instability waves and the origin of bubbles in fluidized beds—II. Comparison with theory. *Int. J. Multiphase Flow* **6,** 305–318.

JACKSON, R. 1985 Hydrodynamic stability of fluid–particle systems In *Fluidization* (Edited by DAVIDSON, J. F., CLIFT, R. & HARRISON, D.), Chap. 2. Academic Press, New York.

KYNCH, G. L. 1952 A theory of sedimentation. *Trans. Faraday Soc.* **48,** 166–176.

KYTÖMAA, H. K. 1987 Stability of the structure in multicomponent flows. Ph.D. Thesis, California Inst. of Technology, Pasadena.

KYTÖMAA, H. K. & BRENNEN, C. E. 1988 Some observations of flow patterns and statistical properties of three component flows. *J. Fluids Engng* **110,** 76–84.

MATUSZKIEWICZ, A., FLAMAND, J. C. & BOURÉ, J. A. 1987 The bubble–slug flow pattern transition and instabilities of void-fraction waves. *Int. J. Multiphase Flow* **13,** 199–217.

MERCADIER, Y. 1981 Contribution à l'étude des propagations de perturbations de taux de vide dans les écoulements diphasiques eau-air à bulles. Ph.D. Thesis, Univ. Scientific et Médicale et Inst. National Polytechnique de Grenoble.

PAUCHON, C. & BANERJEE, S. 1986 Interphase momentum interaction effects in the averaged multifield model. Part I: void propagation in bubbly flows. *Int. J. Multiphase Flow* **12,** 559–573.

PAUCHON, C. & BANERJEE, S. 1987 Interphase momentum interaction effects in the averaged multifield model. Part II: kinematic waves and interfacial drag in bubbly flows. In *ANS Proc. 1987 natn. Heat Transfer Conf.*, Pittsburgh, Pa, pp. 163–171.

SAIZ-JABARDO, J. M. & BOURÉ, J. A. 1989 Experiments on void fraction waves. *Int. J. Multiphase Flow* **15,** 483–493.

TOURNAIRE, A. 1987 Détection et étude des ondes de taux de vide en écoulement diphasiques à bulles jusqu'à la transition bulles–bouchon. Ph.D. Thesis, Univ. Scientific et Médicale et Inst. Nationale Polytechnique de Grenoble.

WALLIS, G. B. 1969 *One Dimensional Two-phase Flow.* McGraw-Hill, New York.

ZENZ, F. A. 1971 In *Fluidization* (Edited by DAVIDSON, J. F. & HARRISON, D.). Academic Press, New York.

ZUBER, N. & FINDLAY, J. A. 1965 Average volumetric concentration in two-phase flow systems. *Trans. ASME J. Heat Transfer* **87C,** 453–468.

ZUBER, N. & STAUB, F. W. 1966 The propagation of wave form of the vapor volumetric concentration in boiling forced convection systems under oscillatory conditions. *J. Heat Transfer* **9,** 871–895.